Atomic structures and covalent-to-metallic transition of lead clusters Pb_n ($n=2$–22)

Baolin Wang,[1,3,5,*] Jijun Zhao,[2,†] Xiaoshuang Chen,[3] Daning Shi,[4] and Guanghou Wang[5]
[1]*Department of Physics, Huaiyin Institute of Technology, Jiangsu 223001, People's Republic of China*
[2]*Department of Physics and Astronomy, University of North Carolina at Chapel Hill, Chapel Hill, North Carolina 27599-3255, USA*
[3]*National Laboratory for Infrared Physics, Shanghai Institute of Technical Physics, Chinese Academy of Sciences, 224502, People's Republic of China*
[4]*Department of Physics, Nanjing University of Aeronautics and Astronautics, Nanjing, 210016, People's Republic of China*
[5]*National Laboratory of Solid State Microstructures and Department of Physics, Nanjing University, Nanjing 210093, People's Republic of China*
(Received 17 October 2004; published 4 March 2005)

The lowest-energy structures and electronic properties of the lead clusters are studied by density-functional-theory calculations with Becke-Lee-Yang-Parr gradient correction. The lowest-energy structures of Pb_n ($n=2$–22) clusters are determined from a number of structural isomers, which are generated from empirical genetic algorithm simulations. The competition between atom-centered compact structures and layered stacking structures leads to the alternative appearance of the two types of structures as global minimum. The size evolution of geometric and electronic properties from covalent bonding towards bulk metallic behavior in Pb clusters is discussed.

DOI: 10.1103/PhysRevA.71.033201 PACS number(s): 36.40.Mr, 36.40.Cg, 61.46.+w

I. INTRODUCTION

During the past decade, the clusters of group-IV elements have been intensively studied [1–34]. It is of fundamental importantance to elucidate the transition from microscopic molecular states to macroscopic solid character. Compared with the comprehensive understanding of silicon [2–9] and germanium clusters [6,10–14], our knowledge on the heavier lead clusters is more restricted. It is known that the bulk lead solid is metallic, in contrast to the bulk silicon and germanium semiconductor crystals. Thus it is particularly interesting to exploit whether the small lead cluster is semimetallic or metallic. Furthermore, if the small lead clusters are semimetallic with covalent bonding like Si_n and Ge_n clusters, at which size will the lead clusters become metallic?

Previous experimental works on lead clusters include dissociation energies [15], mass spectra [16–18], ionization potentials (IPs) [19], photoelectron spectroscopy and electron affinity (EA) [20,21], chemical reactivity [22,23], and injected ion drift tube measurements [24].

On the theoretical side, accurate first-principles calculations on Pb_n clusters are limited in small size, i.e., within $n \leqslant 10$ [25–29]. Larger Pb_n clusters with more than ten atoms have only been studied by spherically averaged pseudopotential calculations [30], semiempirical calculations based on MNDO approximation [31], and empirical many-body potentials [32,33]. Therefore an unbiased structural minimization incorporated with first-principles calculations are essential to understand the bonding character and to illustrate the transition towards metallic behavior of lead clusters. In this work, we perform density-functional calculations on the Pb_n ($n=2$–22) clusters. The geometric structures and size-dependent electronic properties are discussed. An interesting coexistence and competition of two structural growth patterns, i.e., prolate layered structures, more-spherical atom-centered compact structures, is found in the size range of $n=14$–22. A transition from layered structure to atom-centered compact structure is found at Pb_{19}, implying a covalent-to-metallic transition.

II. THEORETICAL METHOD

In this work, electronic structure calculations on Pb_n ($n=2$–22) clusters have been performed by using the density-functional DMOL package [35]. The density functional is treated with Becke's [36] gradient-corrected exchange potential and Lee-Yang-Parr gradient-corrected correlation potential (BLYP) [37]. The effective core potential considering only the valence electrons of Pb [38] and the well-optimized double numerical basis including *d*-polarization function (DND) [35] are chosen.

To search the global minimum structure of lead clusters, we combined an empirical genetic algorithm (GA) simulation [14,39–44,46] with local optimization at BLYP level. The essential purpose in empirical GA simulations is to divide the potential-energy surface (PES) into a number of regions and find a locally stable isomer to represent each region. Although these isomers may not be described very accurately by empirical total-energy models used in GA, the minima from empirical simulation might make a reasonable sampling of the PES and will be further optimized by first-principles density-functional calculations (DFT) calculations. In the GA global optimization, the PES of lead clusters is approximated by a many-body empirical potential [45] fitted for bulk lead solid as well as a semiempirical tight-binding total-energy model fitted for germanium [13] with a uniform rescaling of bond length. The efficiency and validity of the empirical–first-principles hybrid scheme were demonstrated

*Email address: hyblwang@pub.hy.jsinfo.net
†Corresponding author. Email address: zhaojj@mailaps.org

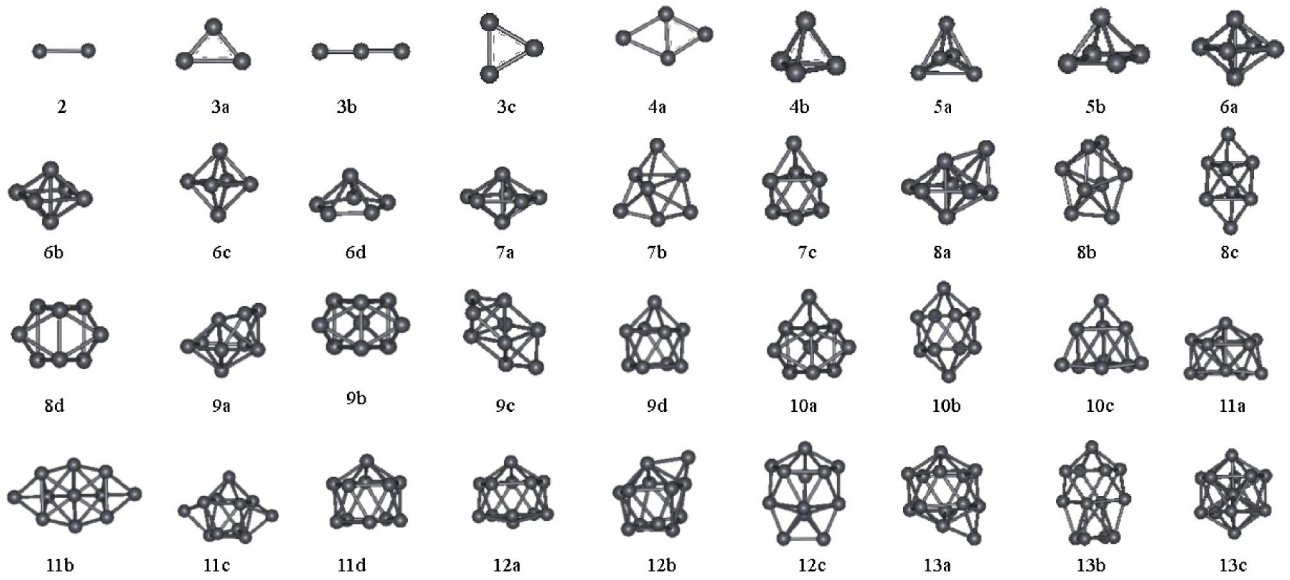

FIG. 1. Lowest-energy structures and metastable isomers for Pb_n ($n=2$–13) clusters.

in our previous works [14,41–44]. The details of GA can be found in our early publications [14,40–44] and recent review [46]. The lowest-energy structures of atomic clusters have been obtained at the BLYP accuracy level up to medium-size, i.e., $n=22$, in this work.

III. LOWEST-ENERGY STRUCTURES OF LEAD CLUSTERS

A. Smaller Pb_n cluster with $n \leqslant 13$

The lowest-energy structures and some representative metastable isomers obtained for neutral Pb_n clusters are presented in Fig. 1 for $n=2$–13 and Fig. 2 for $n=14$–22 and our main theoretical results are summarized in Table I. From our BLYP calculations, the bond length, binding energy, and vibration frequency obtained for lead dimer is 3.07 Å, 1.43 eV, and 111.1 cm^{-1}, respectively. As compared with experimental results (2.93 Å, 0.86 eV, 110 cm^{-1}), the bond length and vibration frequency are well reproduced, while the binding energy is overestimated.

For the Pb_2 dimer, we have examined the effect of basis set, effective core potential, and GGA functional [e.g., Perdew-Wang 1991 (PW91) instead of BLYP] on the theo-

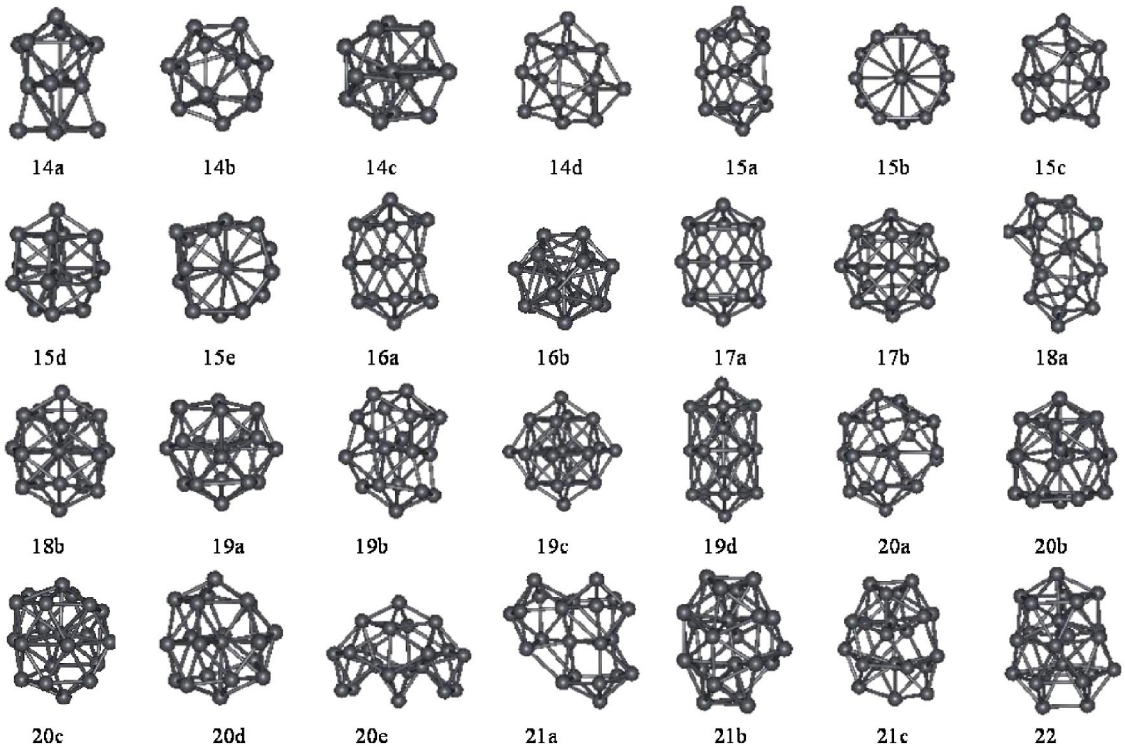

FIG. 2. Lowest-energy structures and metastable isomers for Pb_n ($n=14$–22) clusters.

TABLE I. Lowest-energy configurations and electronic properties of Pb_n clusters. E_b (eV): binding energy per atom; Δ (eV): HOMO-LUMO gap.

n	Geometry	Eb	Δ
2	dimer	0.72	1.49
3	isosceles triangle	1.28	0.70
4	planar rhombus	1.66	1.13
5	trigonal bipyramid	1.72	1.50
6	distorted octahedron	1.85	1.32
7	pentagonal bipyramid	1.95	1.15
8	capped pentagonal bipyramid	1.92	1.07
9	bicapped pentagonal bipyramid	1.98	1.22
10	tetracapped trigonal prism	2.00	1.34
11	distorted incomplete icosahedron	1.97	0.81
12	distorted icosahedron cage	2.00	1.08
13	face-capped icosahedron cage	1.99	0.76
14	layered structure	1.99	0.98
15	layered structure	1.99	0.78
16	layered structure	2.01	1.13
17	layered structure	2.00	0.79
18	layered structure	2.00	0.78
19	atom-centered close-packed	1.98	0.96
20	near-spherical compact structure	1.99	0.74
21	stacked layered structure	1.99	0.69
22	compact and stacked structure	1.98	1.01

retical binding energy. We found that the overestimation of binding energy is a universal feature and is independent of the choice of computational settings. Compared to the experimental binding energy of other group-IV dimers like Si_2 (3.21 eV), Ge_2 (2.65 eV), and Sn_2 (2.04 eV), the binding energy of Pb dimer as 0.86 eV is significantly low. We argue that the Pb_2 dimer is somewhat weakly bonded like those divalent metal dimers such as Cd_2 [41] and Zn_2 [44]. It is known that the DFT calculation cannot reproduce the weak bonding very well. On the other hand, we have also computed the binding energy for fcc solid of Pb. The theoretical binding energy is 2.09 eV/atom, which agrees well with experimental data 2.03 eV/atom. Thus we expect that our theoretical binding energy will become closer to experiments as cluster size increases.

The minimum-energy structure found for Pb_3 is an isosceles triangle (C_{2v}) with bond length 2.94 Å and apex angle $\theta = 80.6°$. It is energetically lower than the equilateral triangle structure (bond length: 3.15 Å) by 0.37 eV and than the linear chain (bond length: 2.87 Å) by 0.12 eV.

The ground-state structure of lead tetramer is a planar rhombus (D_{2h}), which has lower energy ($\Delta E = 1.03$ eV) than a tetrahedron. The side length 3.11 Å and diagonal length 3.33 Å compare well with the bond length 3.04 and 3.23 Å from previous multireference single- and double-excitation configuration interaction (MRSDCI) calculations [17].

The lowest-energy structure found for Pb_5 is a trigonal bipyramid (D_{3h}). The energy of structure is lower than a square bipyramid by 0.63 eV and a planar edge capped rhombus by 0.83 eV. The Pb-Pb distance in the trigonal bipyramid is 3.11 and 4.22 Å, which are comparable to previous MRSDCI results as 3.02 and 4.04 Å [18].

A face-capped trigonal bipyramid is obtained for Pb_6 as lowest-energy structure (6a). This structure is found to be energetically close to a tetragonal bipyramid (6b) by $\Delta E = 0.12$ eV. This lowest-energy structure can also be viewed as a distorted octahedron, which is lower in energy than a perfect octahedron (6c) by 0.98 eV. The pentagonal pyramid (6d) is found energetically close to the perfect octahedron by 0.04 eV.

In the case of Pb_7, we find a pentagonal bipyramid with D_{5h} symmetry (7a) as ground state. It is energetically lower than a face-capped pentagonal bipyramid (7b) by 0.64 eV and a face-capped octahedron (7c) by 0.9 eV. A capped distorted pentagonal bipyramid is found for Pb_8. It is more stable than the isomer (8b) with D_{2h} symmetry by 0.15 eV, than a bicapped octahedron with D_{3h} symmetry (8c) by 0.71 eV, and than a bicapped trigonal prism structure with C_{2v} symmetry (8d) by 0.87 eV. For Pb_9, the ground-state structure is a bicapped pentagonal bipyramid. Its energy is lower than that of a tricapped trigonal prism (D_{3h}, 9b) by 0.6 eV and that of a tricapped octahedron (9c) by 0.78 eV. A capped square antiprism with C_{4v} symmetry (9d) has a higher energy by 1.11 eV isomer. The most stable geometries for Pb_8 and Pb_9 are capped pentagonal bipyramid and bicapped pentagonal bipyramid, respectively. The geometries of Pb_8 and Pb_9 can be easily understood by the growth sequence on the basis of Pb_7. Thus it is not surprising that Pb_7 is more stable than Pb_8 and Pb_9 clusters, as we will show in the latter discussions.

Tetracapped trigonal prism with C_{3v} symmetry is obtained as ground state configuration for Pb_{10}, which is energetically lower than a square bipyramid (D_{4h}, 10b) by 0.52 eV and a tetracapped octahedron (T_d, 10c) by 0.7 eV. The higher geometric symmetry and the larger highest occupied molecular orbital (HOMO)–lowest unoccupied molecular orbital (LUMO) gap [1.34 eV, see Table I and Fig. 3(c)] obtained for Pb_{10} is consistent with the electron shell model that the metal cluster with 40 valence electrons should represent a major shell closing. Thus Pb_{10} cluster is expected to be a highly inert and stable cluster. The present ground-state structures obtained for Pb_{2-10} compare well with previous DFT calculations [29]. These structures of small Pb_n clusters with $n = 3$–10 are similar to the ground-state structures obtained for Si_n [2,5,6] and Ge_n clusters [13,14] implying those smaller lead clusters are covalent bonded.

The lowest-energy structure of Pb_{11} is an atom-centered incompleted icosahedron. This structure can also be viewed as interpenetrating pentagonal bipyramids. Such high compactness is a typical characteristic due to metallic bonding, implying that the smaller lead cluster of this size starts to exhibit some metalliclike behavior. The metastable isomers are the shuttlelike structure (11b), tricapped square antiprism (11c), and uncompleted icosahedron cage (11d) with the total binding-energy difference by $\Delta E = 0.58$, 0.62, and 0.80 eV, respectively. Starting from $n \geqslant 11$, the atom-centered close-packed structures with metalliclike characteristic are always found as locally stable minima for the lead clusters.

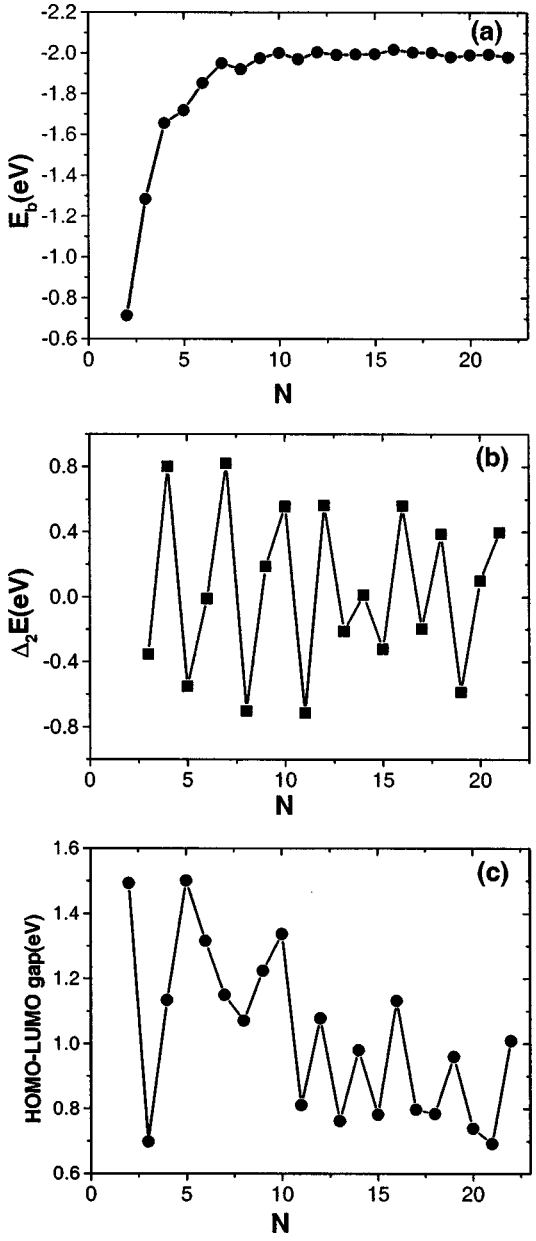

FIG. 3. (a) Binding energy per atom versus cluster size for Pb_n; (b)second difference of cluster energies as a function of cluster size (eV) for $n=2$–22; (c) HOMO-LUMO gap (eV) versus cluster size n.

It is interesting to note that close-packed icosahedral structures are not found to be the lowest-energy structure for Pb_{12} and Pb_{13} clusters. For Pb_{12}, the most stable structure is a strongly distorted icosahedral cage, which has been obtained for Ge_{12} [14]. The metastable isomers are the face-capped distorted cage (12b) and the 1-5-4-2 layered structure (12c). For Pb_{13}, a face capped icosahedron cage (13a) is more stable than the 1-4-4-4 structure (13b) and the perfect atom-centered icosahedron (13c). These results indicate that the high compactness is not the only factor to dominate the cluster geometry of Pb_n at this size range and the bonding of Pb_n clusters still possess certain semimetallic characteristics.

B. Pb_n clusters with $n=14$–22

The lowest-energy structures and some representative metastable isomers obtained for Pb_n ($n=14$–22) are presented in Fig. 2. The lowest-energy structures of Pb_n ($n=14$–17) follow a prolate pattern with stacks of small subunits that form layered structures. The 1-5-4-4, 1-5-3-5-1, 1-5-4-5-1, and 1-5-5-5-1 layered structures obtained the lowest-energy states for Pb_{14}, Pb_{15}, Pb_{16}, and Pb_{17}, respectively. The layered structures have also been found in medium-sized silicon and germanium clusters by previous works [14,7]. The similarity of equilibrium structures for Pb_n, Ge_n, and Si_n clusters at the size range of $n=14$–17 implies that formation of layers with four- or five-member rings is the dominant growth pattern of the medium-sized group-IV elements clusters and the Pb_n ($n=14$–17) clusters are covalent bonded. On the other hand, the more-spherical compact structures are found to be the metastable isomers for Pb_n ($n=14$–18). Indeed, the energies of these metalliclike compact isomers, such as (15b), (16b), (17b), and (18b) in Fig. 2, are rather close to those global minima of the layered structures by $\Delta E=0.07$, 0.64, 0.16, and 0.37 eV, respectively.

However, the layered stacking structural pattern does not continue at Pb_{18}, different from Ge_{18} and Si_{18} clusters. Instead, the lowest-energy structure of Pb_{18} consists of two interpenetrated subunits that form a compact structure. An atom-centered compact structure is obtained for the ground states of Pb_{19}, while the nearly degenerate isomer of Pb_{19} (19 b) is a layered structure by $\Delta E=0.05$ eV only. Other metastable isomers are the ideal fcc-like close-packed octahedron (19c, O_h symmetry) and double icosahedrons (19d, D_{5h} symmetry) by $\Delta E=0.57$ and 1.32 eV, respectively. A cagelike structure with relatively high compactness is obtained as the ground state of Pb_{20}. Compact structures are found as metastable isomers of Pb_{20}, as shown in (20b), (20c), (20d), and (20e) in Fig. 2. The most stable configuration for Pb_{21} is found as a stack of three isomers of Pb_9 (9 d), which is similar to that obtained for Ge_{20} and Ge_{21} [14]. Two metastable isomers of Pb_{21} as (21b) and (21c) in Fig. 2 are atom-centered spherical structures. The more-spherical structure appears again as the lowest-energy state of Pb_{22}.

As the cluster size approach $n=20$, the PES of cluster is rather complicated. Thus our present structures are not guaranteed to be the lowest-energy ones. However, our theoretical calculations clearly reveal a competition between atom-centered compact spherical structures and layered stacking structures in the medium-sized lead clusters. It is interesting to find the alternative appearance of these two kinds of structures that correspond to metallic and semimetallic characteristics, respectively. The similarity between the ground-state structures of Pb_n, Si_n, and Ge_n in the size range we studied implies that the Pb_n clusters with up to 20 atoms are more or less still covalent, although some metallic behaviors characterized by the compact structures are also observed.

In a previous experiment using injected ion drift tube technique [24], it was found that the cationic Pb_n^+ cluster remains near spherical over the experimental size range ($N\simeq 10$–35). Our current theoretical results on lowest-energy structures for Pb_n with $n=10$–22 generally agree with the

experimental observation except at the middle size region of $n=14$–18. Similar to semiconducting Si_n and Ge_n clusters, we find a prolate growth pattern for medium-sized Pb_n clusters of $n=14$–18. However, for $n=14$–17, near-spherical structures were found as metastable isomers whose energy is close to the prolate ones. Moreover, the discrepancy between theory and experiment might also be partially due to the fact that the experiments were carried out on cationic clusters Pb_n^+. The addition of a positive charge on the neutral clusters can induce structural transformation between prolate and near-spherical isomers.

IV. ELECTRONIC PROPERTIES OF LEAD CLUSTERS

The binding energy per atom E_b of the ground states of Pb_n clusters as a function of cluster size n is plotted in Fig. 3(a). The cluster binding energy increases with cluster size n rapidly up to $n<8$ and its size dependence becomes smooth at $n=10$–22. Such behavior can be related to the observed structural transition around $n=10$–13. The equilibrium geometries undergo a transition from near-spherical structure to prolate geometry at $n=14$. Our present results on the size dependence of the binding energy of Pb_n is similar to the results of Ge_n [14] and Zn_n [44] clusters in our previous DFT calculations.

We plot the second difference of total energies defined by $\Delta_2 E=E(n+1)+E(n-1)-2E(n)$ in Fig. 3(b), which is a sensitive quantity that characterizes the stability of cluster, as a function of cluster size. Local maximum peaks for $\Delta_2 E$ are found at $n=4$, 7, 10, 12, 14, 16, 18, and 21, indicating that the cluster with these values of n might be more stable than their neighboring clusters. Previous experiments have recorded the mass spectra of anionic or cationic lead clusters and found the "magic numbers" as peaks of the cluster abundance at $n=7$, 10, 13, 15, 17, 19 for Pb_n^+ [16–18] and at $n=7$, 10, and partly 15 for Pb_n^- [20]. Compared with experiments, the two major magic numbers at $n=7$ and 10 for both cationic and anionic clusters are well reproduced by our calculations, while the discrepancy in other sizes might be attributed to the different charge states in experiments and theoretical calculations. It is also noteworthy that $n=4$, 7, and 10 were found to be the magic numbers for small Si_n and Ge_n clusters from most of the previous calculations. Again, this similarity indicates that the small lead clusters are covalent bonded like Si_n and Ge_n.

In Fig. 3(c), we present the energy gap between the highest occupied molecular orbital (HOMO) and lowest unoccupied molecular orbital (LUMO) for the lowest-energy state of Pb_n ($n=2$–22) clusters. Generally, higher-energy gap should make the clusters to be more stable and more abundant. The HOMO-LUMO gap is relatively higher for Pb_n with $n=2$, 5, 10, 12, 14, 16, 19, and 22, respectively. Indeed, Pb_2, Pb_5, and Pb_{10} with 8, 20, and 40 valence electrons correspond to the major shell closing of electron shell model. Particularly, the ground-state Pb_{10} cluster has a HOMO-LUMO gap as high as 1.34 eV and a higher symmetry (C_{3v}). On the other hand, a larger energy gap also is found in Pb_{12}, Pb_{14}, Pb_{16}, Pb_{19}, and Pb_{22} clusters without the major closed-shell electronic configuration. The coincidence between the maxima for second difference of total energies and HOMO-LUMO gap (e.g., $n=10$, 12, 14, 16) also implies that relative stability of the lead clusters is dominated by electron effect instead of geometry packing. In Fig. 3(c), the HOMO-LUMO gap of Pb_n generally decreases as cluster size n increases, indicating a trend of covalent-to-metallic transition. However, for all Pb_n clusters studied, their HOMO-LUMO gaps are still higher than 0.6 eV up to $n=22$. This result further supports our previous argument that the Pb_n clusters with up to 20 atoms are still mostly covalent.

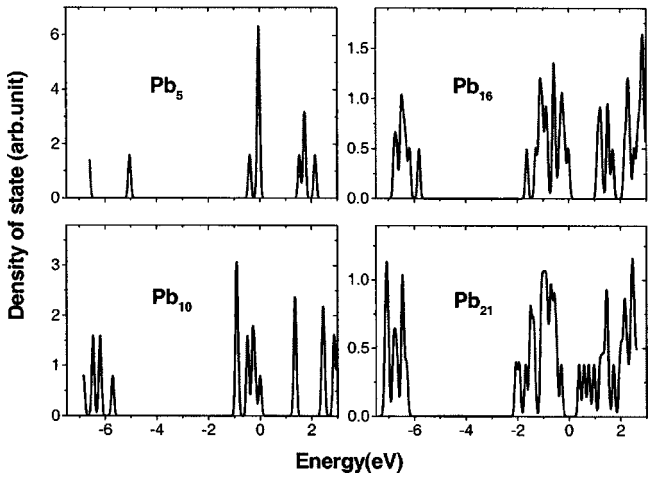

FIG. 4. Density of states (DOS) of the Pb_5, Pb_{10}, Pb_{16}, and Pb_{21} clusters. The Fermi level is set as zero. Gaussian broadening of 0.05 eV is used.

We further investigate the size evolution electronic properties of lead clusters by examining the electronic density of states (DOS) of several representative lead clusters: Pb_5, Pb_{10}, Pb_{16}, and Pb_{21}. As shown in Fig. 4, the energy levels for cluster Pb_5 are discrete, and the *d* and *sp* peaks are clearly separated. The DOS of Pb_{10} is still sparse and discrete although the *d* and *sp* energy levels are gradually broadened. As cluster size further increases, the *d* and *sp* levels broaden, shift, and overlap with each other. Thus continuouslike electronic bands are found in Pb_{16} and Pb_{21}.

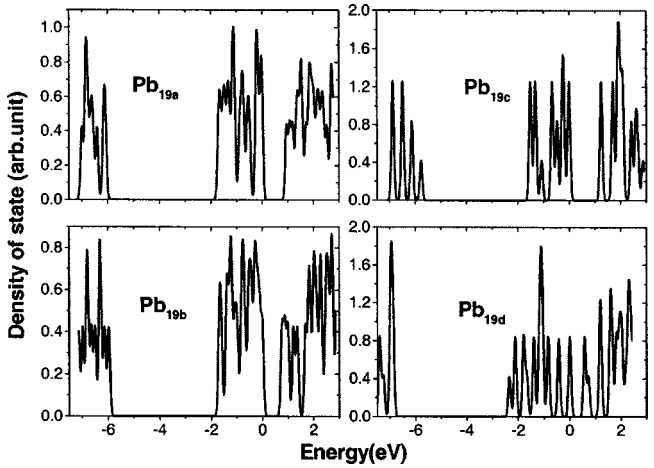

FIG. 5. Density of states (DOS) of the Pb_{19} with different geometries. The Fermi level is set as zero. Gaussian broadening of 0.05 eV is used.

To explore the geometry effect on the electronic structure, we compare the electronic density of states (DOS) of Pb_{19} for the four isomers: atom-centered spherical structure; layered stacking structure; fcc-like close-packed octahedron; double icosahedron, as shown in Fig. 5. The cluster electronic DOS shows remarkable structural sensitivity. The DOS for atom-centered spherical structure (Pb_{19a}) present three isolated bands with small energy gap between the conduct and valence bands. DOS for layered structure (Pb_{19b}) displays more uniform distributions in comparison with the Pb_{19c} and Pb_{19d}, which have the higher symmetry. The DOS of double icosahedrons (Pb_{19d}) shows continuous electronic bands at Fermi energy without the energy gap between the conduction- and valence-band distributions as is evident of metallic nature. Such structural dependence of electronic state can be used to identify the cluster geometries with the aid of experimental spectroscopic measurements. In previous works, the theoretical DOS were compared with experimental photoelectron spectra for clusters like Si_n and Al_n [4,47].

V. CONCLUSION

In summary, we have studied the structural and electronic structures of Pb_n ($n=2$–22) clusters by using BLYP calculation combined with an empirical genetic algorithm simulation. The main conclusions can be drawn in the following points. (i) The structures of smaller Pb_n ($n \leqslant 10$) clusters are similar to those of Si and Ge clusters. Lead clusters follow a prolate growth pattern starting from $n=14$. The layered stacking structures are dominant in the size range of $n=13$–18. However, an atom-centered compact structure is found in Pb_{19}, and there is competition between the atom-centered compact structure and the layered stacking structure. (ii) The size dependence of binding energy, second difference of binding energy, and HOMO-LUMO gap are discussed for the Pb_n clusters. Our results indicated that the clusters with $n=4$, 7, 10, 12, 16, 18, 21 are more stable than their neighboring clusters. The relative stability of the Pb_n clusters is mostly associated to the electron effect instead of geometry packing effect. (iii) The covalent-to-metallic transition starts from Pb_{11}, while the Pb_n cluster with about 20 atoms still has a finite gap of $\sim$1eV and can still be considered as semimetallic cluster with covalent bonding. Further study on the larger lead clusters with $n \geqslant 20$ to reveal the transition into metallic bonding is still under way.

ACKNOWLEDGMENTS

The authors would like to thank the National Natural Science Foundation of China (Grant Nos. 29890210, 10372045), the National Climbing Project of China, the Foundation for the Author of National Excellent Doctoral Dissertation of P.R. China (FANEDD), and the program for New Century Excellent Talents in University of P.R. China for financial support.

[1] *Clusters of Atoms and Molecules I*, edited by H. Haberland (Springer-Verlag, Berlin, 1995).
[2] K. Raghavachari and C. M. Rohlfing, J. Chem. Phys. **89**, 2219 (1988).
[3] M. F. Jarrold and V. A. Constant, Phys. Rev. Lett. **67**, 2994 (1991).
[4] N. Binggeli and J. R. Chelikowsky, Phys. Rev. Lett. **75**, 493 (1995).
[5] B. Liu, Z. Y. Lu, B. Pan, C. Z. Wang, K. M. Ho, A. A. Shvartsburg, and M. F. Jarrold, J. Chem. Phys. **109**, 9401 (1998).
[6] Z. Y. Lu, C. Z. Wang, and K. M. Ho, Phys. Rev. B **61**, 2329 (2000).
[7] K. M. Ho, A. A. Shvartsburg, B. Pan, Z. Y. Lu, C. Z. Wang, J. G. Wacker, J. L. Fye, and M. E. Jarrold, Nature (London) **392**, 582 (1998).
[8] K. A. Jackson, M. Horoi, I. Chaudhuri, T. Frauenheim, and A. A. Shvartsburg, Phys. Rev. Lett. **93**, 013401 (2004).
[9] S. Yoo, J. J. Zhao, J. L. Wang, and X. C. Zeng, J. Am. Chem. Soc.(to be published).
[10] J. M. Hunter, J. L. Fye, M. F. Jarrold, and J. E. Bower, Phys. Rev. Lett. **73**, 2063 (1993).
[11] S. Ogut and J. R. Chelikowsky, Phys. Rev. B **55**, 4914 (1997).
[12] G. R. Burton, C. Xu, C. C. Arnold, and D. M. Meumark, J. Chem. Phys. **104**, 2757 (1996).
[13] J. J. Zhao, J. L. Wang, and G. H. Wang, Phys. Lett. A **275**, 281 (2000).
[14] J. L. Wang, G. H. Wang, and J. J. Zhao, Phys. Rev. B **64**, 205411 (2001).
[15] K. A. Gingerich, D. L. Cocke, and F. Miller, J. Chem. Phys. **64**, 4027 (1976).
[16] J. Muhlbach, P. Pfau, K. Sattler, and E. Recknagel, Z. Phys. B: Condens. Matter **47**, 233 (1982).
[17] K. Laihing, R. G. Wheeler, W. L. Wilson, and M. A. Duncan, J. Chem. Phys. **87**, 3401 (1987).
[18] R. W. Farley, P. Ziemann, and A. W. Castleman, Jr., Z. Phys. D: At., Mol. Clusters **14**, 353 (1989).
[19] Y. Saito, K. Yamauchi, K. Mihama, and T. Noda, Jpn. J. Appl. Phys., Part 2 **21**, L396 (1982).
[20] G. Gantefor, M. Gausa, K. H. Meiwes-Broer, and H. O. Lutz, Z. Phys. D: At., Mol. Clusters **12**, 405 (1989).
[21] Ch. Luder, and K. H. Meiwes-Broer, Chem. Phys. Lett. **294**, 391 (1998).
[22] X. Ren, and K. M. Ervin, Chem. Phys. Lett. **198**, 229 (1992).
[23] R. W. Farley, P. Ziemann, R. G. Keesee, and A. W. Castleman, Jr., Z. Phys. D: At., Mol. Clusters **25**, 267 (1989).
[24] A. A. Shvartsburg, and M. F. Jarrold, Chem. Phys. Lett. **317**, 615 (2000).
[25] G. Pacchioni, Mol. Phys. **55**, 211 (1985).
[26] K. Balasubramanian and K. S. Pitzer, J. Chem. Phys. **78**, 321 (1983).
[27] D. Dai and K. Balasubramanian, J. Chem. Phys. **96**, 8345 (1992).
[28] D. Dai, and K. Balasubramanian, Chem. Phys. Lett. **271**, 118

(1997).
[29] B. Wang, L. M. Molina, M. J. Lopez, A. Rubio, J. A. Alonso, and M. J. Stott, Ann. Phys. **7**, 107 (1998).
[30] M. P. Iniguez, M. J. Lopez, J. A. Alonso, and J. M. Soler, Z. Phys. D: At., Mol. Clusters **11**, 163 (1989).
[31] A. M. Mazzone, Phys. Rev. B **54**, 5970 (1996).
[32] J. P. K. Doye and S. C. Hendy, Eur. Phys. J. D **22**, 99 (2003).
[33] S. K. Lai, P. J. Hsu, K. L. Wu, W. K. Liu, and M. Iwamatsu, J. Chem. Phys. **117**, 10715 (2002).
[34] A. A. Shvartsburg and M. F. Jarrold, Phys. Rev. A **60**, 1235 (1999).
[35] DMOL is a density-functional-theory (DFT) package-based atomic basis distributed by MSI [B. Delley, Phys. Rev. A **92**, 508 (1990)].
[36] A. D. Becke, Phys. Rev. A **38**, 3098 (1988).
[37] C. Lee, W. Yang, and R. G. Parr, Phys. Rev. B **37**, 785 (1988).
[38] M. Dolg, U. Wedig, H. Stoll, and H. J. Preuss, J. Chem. Phys. **86**, 866 (1987); A. Bergner, M. Dolg, W. Kuechle, H. Stoll, and H. J. Preuss, Mol. Phys. **80**, 1431 (1993).
[39] D. M. Deaven and K. M. Ho, Phys. Rev. Lett. **75**, 288 (1995).
[40] Y. H. Luo, J. J. Zhao, S. T. Qiu, and G. H. Wang, Phys. Rev. B **59**, 14903 (1999); J. J. Zhao, Y. H. Luo, and G. H. Wang, Eur. Phys. J. D **14**, 309 (2001).
[41] J. J. Zhao, Phys. Rev. A **64**, 043204 (2001).
[42] J. L. Wang, G. H. Wang, and J. J. Zhao, J. Phys.: Condens. Matter **13**, L753 (2001).
[43] J. L. Wang, G. H. Wang, and J. J. Zhao, Phys. Rev. B **66**, 035418 (2002).
[44] J. L. Wang, G. H. Wang, and J. J. Zhao, Phys. Rev. A **68**, 013201 (2003).
[45] F. Cleri and V. Rosato, Phys. Rev. B **48**, 22 (1993).
[46] J. J. Zhao and R. H. Xie, J. Comput. Theor. Nanosci. **1**, 117 (2004).
[47] J. Akola, M. Manninen, H. Hakkinen, U. Landman, X. Li, and L. S. Wang, Phys. Rev. B **62**, 13 216 (2000).